crystals

MDPI

Article

Effect of Heat Treatment on the Structural-Phase State and Properties of a Multilayer Co-Cr-Al-Y Coating

Mazhyn Skakov [1,2], Assel Zhilkashinova [1,*], Almira Zhilkashinova [1,*], Madi Abilev [1,3], Nadezhda Prokhorenkova [1,4], Maksut Agelmenev [5] and Akmaral Ismailova [3]

1 National Research Laboratory for Collective Use, Sarsen Amanzholov East Kazakhstan University, 34 Tridtsatoy Gvardeiskoy Divizii Street, Ust-Kamenogorsk 070002, Kazakhstan; skakovmk@mail.ru (M.S.); m.abilev@mail.ru (M.A.); nadin_kaz@mail.ru (N.P.)
2 Science Department, National Nuclear Center of the Republic of Kazakhstan, 2 Krasnoarmeyskaya Street, Kurchatov 071100, Kazakhstan
3 Department of Analytical, Colloid Chemistry and Technology of Rare Elements, Al-Farabi Kazakh National University, 71 Al-Farabi Avenue, Almaty 050040, Kazakhstan; makon72@mail.ru
4 School of Traditional and Alternative Energy, D. Serikbayev East Kazakhstan Technical University, 69 Protozanov Street, Ust-Kamenogorsk 070004, Kazakhstan
5 Department of Physics and Nanotechnology, Karaganda Buketov University, 28 University Street, Karaganda 100024, Kazakhstan; amaxut58@gmail.com
* Correspondence: asssel2462@mail.ru (A.Z.); almira_1981@mail.ru (A.Z.)

Abstract: The article describes the effect of heat treatment on the structural-phase state and properties of a multilayer Cr-Al-Co-Y coating obtained by magnetron sputtering. Heat treatment was carried out at 400, 800 and 1000 °C. The study of the microstructure was carried out by electron microscopy with energy dispersive analysis and powder X-ray diffraction. The surface of the samples was studied by atomic force microscopy. The thickness of the Co-Cr-Al-Y coatings was 1.5–1.7 ± 0.2 μm. The obtained coatings are characterized by a hardness of 4.7–6.4 GPa. A distinctive feature of the layers is the absence of a crystalline structure in some areas of the coating. The main process occurring during the thermal treatment is the formation of a spinel-type phase. For a single-layer sample after heat treatment at 400 °C, it was not possible to fix extraneous reflections except for the reflections of the silicon substrate 111 and 220. For the rest of the samples, the appearance of reflections of a number of phases was noticed, such as: SiO_2, CoO, $AlSi_{0.5}O_{2.5}$ and $CrAl_{0.4}2Si_{1.58}$. An increase in the treatment temperature up to 800 °C did not lead to significant changes. In the case of the multilayer sample, the reflections of various impurity phases disappeared and the Co_3O_4 phase was formed. For samples treated at 1000 °C, the formation of a spinel-type phase (Co_3O_4-$CoCr_2O_4$) was observed in all cases. Data on the structural-phase state and properties of the multilayer Co-Cr-Al-Y coating can be used to predict the nature of such coatings after heat treatment.

Keywords: multilayer Co-Cr-Al-Y coating; heat treatment; magnetron sputtering; microstructure; phase composition

Citation: Skakov, M.; Zhilkashinova, A.; Zhilkashinova, A.; Abilev, M.; Prokhorenkova, N.; Agelmenev, M.; Ismailova, A. Effect of Heat Treatment on the Structural-Phase State and Properties of a Multilayer Co-Cr-Al-Y Coating. *Crystals* **2022**, *12*, 1056. https://doi.org/10.3390/cryst12081056

Academic Editor: Zaoli Zhang

Received: 22 June 2022
Accepted: 23 July 2022
Published: 28 July 2022

1. Introduction

Hot parts of the industrial equipment (combustion chamber, turbine flow path, etc., with surface temperatures more than 850 °C) can work for a long time only if there are special protective coatings on the surface. Conventionally, protective coatings can be divided into two classes: metal heat-resistant coatings for protecting the surface of parts from the corrosion and erosion effects of the working environment (heat-resistant coatings can be single or multilayer, where each layer differs in its chemical composition and thickness); complex heat-protective coatings (HPC) with a ceramic thermal barrier layer, which, along with protecting the surface from the corrosive effects of the environment, reduces the effect of heat flow [1–3]. The most widely used heat-resistant coatings include aluminizing, aluminosilicizing, chromium-aluminizing and multicomponent coatings.

Currently, the search for new thermal barrier coatings is primarily associated with the optimization of the chemical composition of new compositions, with the development and mastering of new technological processes based on the use of fundamentally new physical effects, as well as with the use of newly created coatings [4–6]. The basic system of heat-resistant coatings is Me-Cr-Al, where Me is Fe, Co, or Ni. Such coatings require the creation of strong adhesion, the reproducibility of the composition of the evaporated material in the coatings, the suppression of the droplet component, the exclusion of the columnar structure and the associated through porosity, additional doping of the condensate and the inclusion of diffusion-barrier sublayers in the coating [7–10].

Features of the composition of Me-Cr-Al-Y coatings are due to the following factors: chromium is introduced to prevent high-temperature corrosion, but its use concerns only the effect on the substrate and has an impact on the formation of a coating layer with it [11–13]. Oxidation can be prevented by increasing the aluminum content, but this can also cause a decrease in the ductility of the coating. Yttrium is able to significantly increase the adhesion of the oxide layer due to the formation of rods binding the oxide layer and the coating. However, the main function of using yttrium is its ability to form compounds with sulfur, which do not allow disintegration of the oxide layer. Cobalt in the coating composition significantly increases the resistance to natural oxidation, but it also leads to a decrease in the melting temperature of the blade coating and contributes to an increase in the resistance of the blades to cyclic or isothermal oxidation [14–16].

Methods used to form protective coatings include plasma deposition, diffusion method, magnetron sputtering, plasma arc cathode sputtering, laser method, electron-beam deposition, etc. [6,7,17]. The magnetron sputtering method is widely used to apply industrially significant coatings [18,19]. Magnetron sputtering systems make it possible to set and vary the properties and structures of coatings within the required ranges. Magnetron sputtering is characterized by high repeatability and stability of the deposited coatings both in terms of the sputtering rate and the characteristics of the resulting coatings. This feature of magnetron systems, unlike, for example, electron-beam evaporation, with well-selected modes of deposition of individual layers, makes it possible to obtain rather complex multilayer coatings without a need for a thickness control system. Due to the high energy efficiency and degree of ionization, magnetron sputtering makes it possible to obtain dense layers, which is essential for substrate materials that do not allow heating [18,19].

A large set of corrosion-resistant materials has been developed for magnetron sputtering of the Me-Cr-Al-Y system, which is most widely used as protective coatings under conditions of high-temperature sulfide-oxide corrosion [20]. Me-Cr-Al-Y heat-resistant coatings reduce the temperature of the metal and have low thermal conductivity, low density and withstand cyclic loads [13,21–23]. Me-Cr-Al-R coating of a regulated thickness (60–80 μm) has been developed for working blades of turbine engines with a service life of up to 10,000 h [3,5,8,9]. The studied microstructure of the complex gradient coating in the initial state and after annealing is represented by different phases.

Previously, we have studied composite (Cr-Al-Co + ZrO_2-Y_2O_3) coatings on a Ni-Cr alloy substrate [24]. The coating with a total layer thickness of 17–18 μm was obtained by magnetron sputtering, including an inner layer (Cr-Al-Co) with a thickness of 10–11 μm and an outer ceramic layer (ZrO_2-Y_2O_3) with a thickness of 6–7 μm.

The multifactorial nature of the formation processes of heat-resistant coatings and the variety of causes and mechanisms of their degradation, damage and destruction during operation do not allow choosing a universal protective coating. For each new modification of parts, it is necessary to select a new coating or adjust the technology for applying a known coating. Therefore, the existing compositions of coatings and technological processes for their application are constantly being improved, fundamentally new technologies are being developed and the most effective protection systems are being selected for new heat-resistant alloys and new designs of air-cooled blades, etc.

Along with the chemical composition, one of the most important characteristics of a heat-resistant coating should be considered its structure. The coating structure determines

not only its strength, ductility, fracture toughness, fatigue resistance and other properties but also its main characteristic—heat resistance. Obtaining an optimal structure is an important condition for achieving the required coating properties. Therefore, the development and widespread use of novel effective heat-resistant coatings and progressive fundamentally new technologies for their creation is undoubtedly associated with the need for deep systematic structural studies of these coatings at all stages of their creation and operation. These studies should be aimed at the identification of the general patterns of structure formation and the diffusion interaction of the coating with alloy and with the protective oxide film. The change and degradation of the structure under the influence of a wide variety of external factors, determining the role and mechanisms of influence of a particular alloying element or a complex of such elements on the formation of the structure and properties of the coating during deposition and technological heat treatment should also be studied.

Thus, the main goal of this research was to reveal the changes in the structural-phase state and properties of the composite Co-Cr-Al-Y coating and after the heat treatment.

2. Materials and Methods

The object of the study was Co-Cr-Al-Y coatings. The coatings were deposited on a single-crystal silicon substrate with the [100] crystallographic orientation. Coating was carried out by the magnetron method on an ion-plasma setup, which was a vacuum chamber with two magnetron sputtering systems of an unbalanced type and an ion source with a closed electron drift [24].

The coatings were heat treated on a MILA-5000 unit (ULVAC Technologies Inc., Methuen, MA, USA). This setup was used to heat the samples at 400; 800 and 1000 °C. The heating took place in a programmed mode with a given rate of reaching the desired temperature, as well as during the transition from one temperature to another. The treatment time at a given temperature or sequentially at several temperatures also took place in the programmed mode: for 400 °C—10 min heating, holding for 10 h, cooling, removing after 1 h; for 800 °C and 1000 °C—the same, but heating was for 20 min, not 10 min. The samples were heated under high vacuum (1×10^{-7} mm Hg). Heat treatment of coatings at 400, 800 and 1000 °C was carried out in order to determine the effect of thermal treatment on the structural-phase state and properties of composite coatings. After the annealing process under the selected modes of thermal modification of each sample, the studies described in the article were carried out in order to establish the patterns of changes in the states of the coatings, that is, what changes occurred after annealing at 400, 800 and 1000 °C. Since a system of such coatings can potentially be used for working blades of gas turbine engines, it is necessary to evaluate the structural phase and mechanical properties of such coatings after thermal exposure. The maximum temperature that the studied coatings were subjected to was 1000 °C. This temperature corresponds to the gas temperature at the turbine inlet of currently operated gas turbine engines (the blade metal temperature of 900–1000 °C).

Determination of the structural-phase state and elemental composition by scanning electron microscopy was carried out on a JEOL-2200FS (JEOL, Tokyo, Japan) (EDX) INCA ENERGY scanning electron microscope (Oxford Instruments, Abingdon, UK). The accelerating voltage was up to 30 kV, resolution up to 3 nm and instrumental magnification up to ×300,000. Samples were placed in a mold with a diameter of 30 mm, filled with epoxy filler, dried and then the resulting puck was ground and polished. The morphology was also studied on a Tescan Solaris FE-SEM two-beam scanning electron microscope (TESCAN, Brno, Czech Republic) with an accelerating voltage of 20 kV in secondary electron modes. The device is equipped with an AztecLive (Oxford Instruments, Abingdon, UK) energy-dispersive X-ray characteristic spectrometer (EDX) with a semiconductor Si detector with an energy resolution of 128 eV.

The microstructure of the treated samples was studied using a ThemisZ electron microscope (Thermo Scientific, Waltham, MA, USA) with an accelerating voltage of 200 kV and a

limiting resolution of 0.07 nm. Images were recorded using Ceta 16 CCD array (Thermo Scientific, USA). The instrument is equipped with SuperX (Thermo Fisher Scientific, USA) energy-dispersive X-ray spectrometer (EDX) with a semiconductor Si detector with an energy resolution of 128 eV.

Preparation of a solid-state sample for TEM (preparation of a cross section by grinding with etching) was carried out by applying a scratch with a scriber (Fine Point Diamond Scriber 54467, Ted Pella, Redding, CA, USA) to the substrate on the reverse side of the sample. The gluing of the split pieces takes place with the front sides (films on the substrates), in such a way that two ends become visible. A special epoxy two-part adhesive EpoxyBond 110TM 2-Part Adhesive (Allied High Tech Products Inc., Compton, CA, USA) was used. The gluing was placed under a press, and then the glue solidified by heating in an oven at 130 °C for 15 min. Next, a quartz cylinder with a diameter of 5 mm was used, on the heated surface of which a layer of wax was applied and a gluing of samples from the ends is attached to the wax.

Further, the sample was polished at the LEICA EM TXP grinding and polishing station using four successive grinding wheels. A quartz cylinder with samples glued to it was placed in the holder of the grinding system, and the sample was polished on one side to a thickness of 200 μm. When the sample thickness reached 200 μm, the cylinder was again heated (to heat up the wax), the sample was washed in a cuvette with acetone, and silicon "satellites" were placed on the cylinder, between which there was a gluing of the samples, but already turned over by the other (unpolished) side. After completion of the mechanical grinding procedure, the cylinder with the samples was removed from the instrument holder, satellites were removed from the cylinder, and a 3-mm copper ring was glued on the top of the sample.

Next, the samples were subjected to additional thinning using ion etching. The copper ring with the sample was placed in a special holder for the Gatan Precision Ion polishing system model 691 ion etching station. On the sample, in the place where the deposited coating is located, there will be a rather thin area where the structure through the transmission in TEM could be seen. The sample was transferred to a special sample holder EM-21010/21020: Single Tilt Holder for JEOL-2200FS TEM (JEOL, Tokyo, Japan). The sample holder with the sample was placed in a pre-prepared TEM, with an evacuated chamber, heated nodes and included software. The chamber with the sample is pumped out for about 10 min.

The crack resistance of the coatings was evaluated on an NHT2 nanoindenter (CSM Instruments, Peseux, Switzerland) with a Berkovich diamond indenter. Loading and unloading were carried out at a rate of 20 mN/min, holding under load for 30 s. The Oliver–Pharr method was used to determine the hardness and Young's modulus. This method for evaluating the crack resistance of the coating serves to form radial cracks. On the sample surface, traces of these cracks propagate from the corners of the imprint.

X-ray diffraction phase analysis was performed on Shimadzu XRD 6000 instrument (Shimadzu, Kyoto, Japan) with a Cu Kα anode (λ = 0.154 nm) by the grazing beam method (shooting angle was 15°) in the 2θ range 20–80°. Because of the low intensity of the peaks, the initial signal was approximated by Gaussian curves. Studies were also carried out using the X-ray powder diffraction method on the ARLX'tra instrument (Thermo Fisher Scientific, Waltham, MA, USA). An X-ray tube with a characteristic radiation wavelength λ = 1.5418 Å was used as an X-ray source. The sample before each shooting was fixed with glue on an amorphous polycarbonate cuvette. The shooting of thin film samples was performed using symmetrical (Bragg–Brentano) geometry, in the angle range of 15–70°, and asymmetric geometry, in the range of 20–50° (in some cases, 15–70°). In the case of using asymmetric geometry, the angle between the surface of the sample and the X-ray beam was changed in the range of 1–5°, to analyze the material layer by layer. The step size during the study was 0.05°, and the accumulation time was 3 s at each point. X-ray diffraction phase analysis of the films was performed using the 2θ positions of individual peaks. Phase analysis was

carried out using the CSM "Search-Match" software. The PDF-2 database compiled by the International Committee on Diffraction Data JCPDS (ICDD) was used as a reference file.

The surface morphology of the Co-Cr-Al-Y coatings was recorded using an NTEGRA Prima atomic force microscope (NT-MDT, Moscow, Russia). The shooting area for all samples was 100 × 100 µm.

All the procedures are summarized in Table 1.

Table 1. Research plan.

Procedure	Method
Coating	Magnetron sputtering on Si substrate
Testing	SEM, TEM, XRD, AFM, microhardness
Heating	Treatment at 400, 800 and 1000 °C
Testing after heating	SEM, TEM, XRD, AFM, microhardness

3. Results and Discussion

Studies of the structural-phase state and properties of the Co-Cr-Al-Y coating in the initial state were carried out. Figure 1 shows the load curves of a four-layer coating and an optical photograph of the indentations. The optical image shows that the indentation depth was 360 nm, reaching approximately 24% of the film thickness.

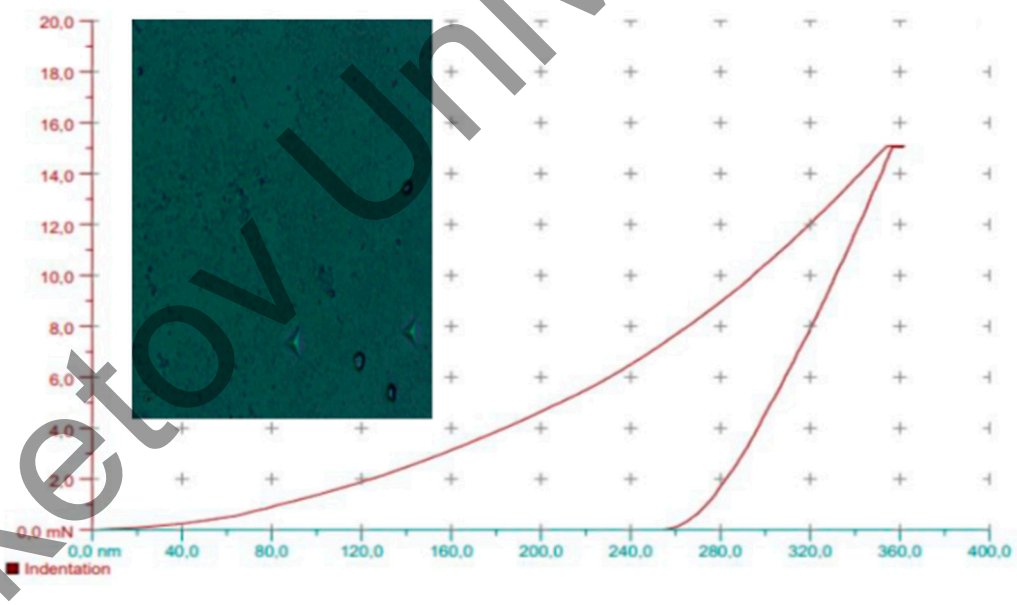

Figure 1. Loading curves of the four-layer coating.

All studied Co-Cr-Al-Y coatings are characterized by a hardness value in the range of 4.7–6.4 GPa, which is the resulting average hardness of the main components of the coating: Co, Cr and Al (Table 2). At the same time, the value of H/E* (E* = E/(1 − ν), H is the hardness of the material, E is the Young's modulus of the material, ν is the Poisson's ratio) is non-linear with a maximum for the four-layer coating (H/E* = 0.048), which makes it the most crack-resistant system of all studied in this research.

Table 2. Microhardness of samples.

Sample	Microhardness, GPa
Single-layer coating	5.60 ± 0.11
Double-layer coating	6.30 ± 0.10
Four-layer coating	6.40 ± 0.10
Eight-layer coating	4.70 ± 0.09

The results of studying the cross section of coatings by scanning electron microscopy and the corresponding energy dispersive spectra are shown in Figure 2.

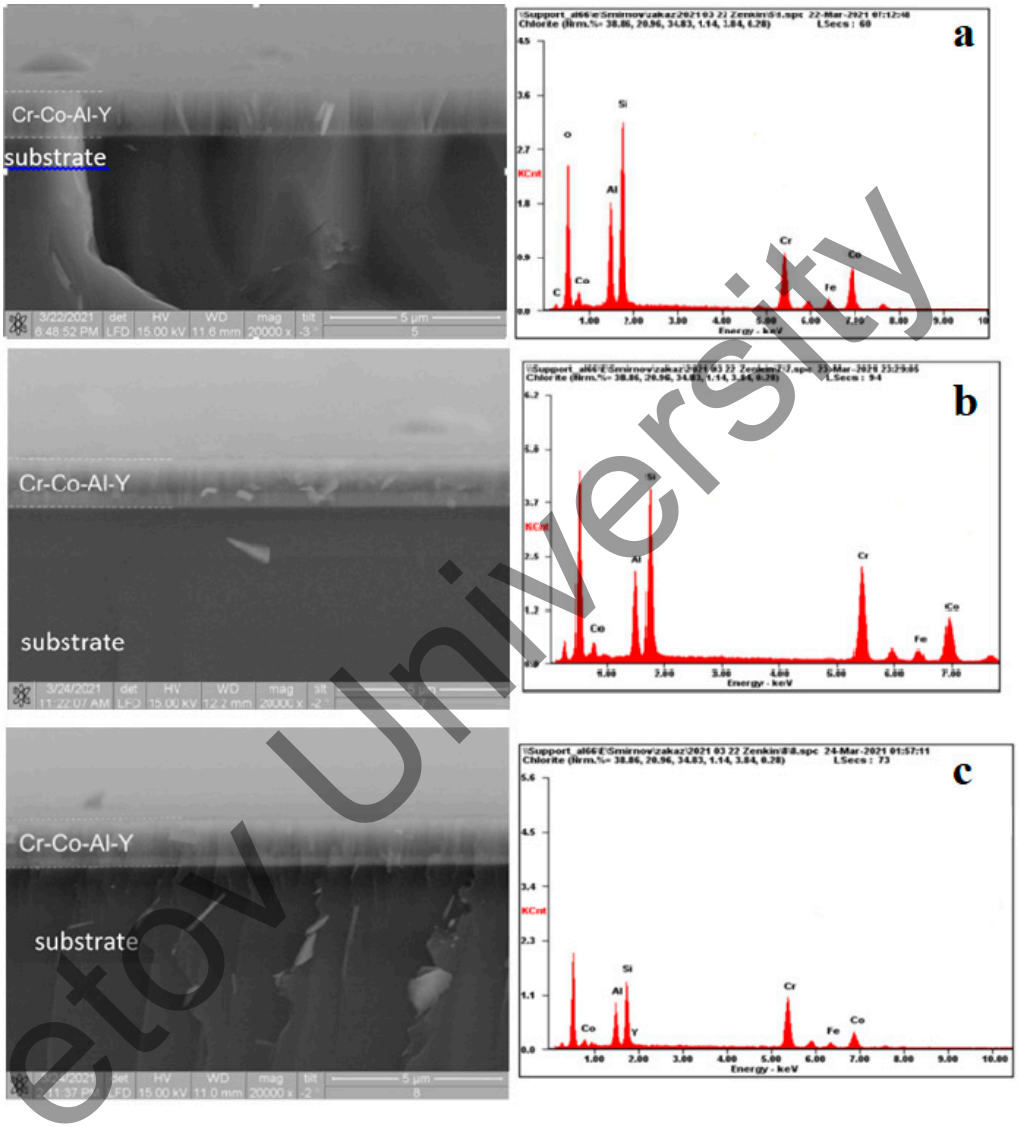

Figure 2. SEM images and energy-dispersive spectra of the cross section of the single-layer coating (**a**), four-layer coating (**b**) and eight-layer coating (**c**).

The thickness of all Co-Cr-Al-Y coatings is 1.7 ± 0.2 µm (Table 3). According to the energy dispersive analysis data, the chromium concentration in the coating increases with an increase in the number of layers, with a proportional decrease for cobalt, which is associated with the influence of the second layer with an increased chromium concentration. The detection of a large amount of silicon is due to the feature of the method and the detection of a signal from the substrate; therefore, it may not be taken into account when measuring the mutual concentrations of the elements of the Co-Cr-Al-Y system. The presence of an oxygen peak in the EDS spectrum is due to its adsorption on the cut surface after removal from the vacuum chamber. In view of the fact that the same group of elements is used in the layers, it is impossible to achieve a clear separation of the layers by scanning microscopy.

Transmission microscopy results confirm the SEM and EDS measurements. TEM images show clear layer boundaries for each type of multilayer coating (Figures 3–5, Table 4). The Co-Cr-Al-Y system forms dense coatings without a pronounced columnar structure characteristic of metal coatings.

Table 3. Averaged R_a, R_z of the Co-Cr-Al-Y coating surface.

Sample	R_a, μm	R_z, μm	Coating Thickness, μm
Single-layer coating	20.3	127	0.3 ± 0.1
Double-layer coating	17.0	121	0.6 ± 0.2
Four-layer coating	26.9	134	1.1 ± 0.2
Eight-layer coating	16.7	101	1.7 ± 0.2

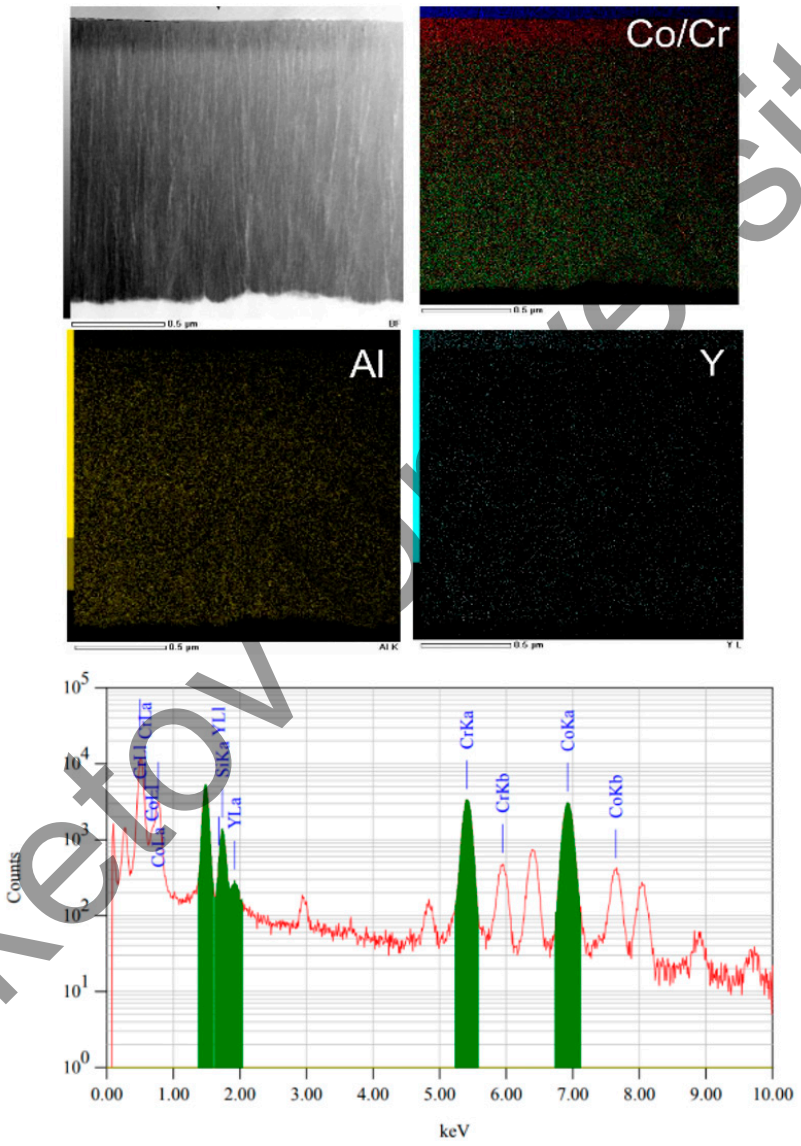

Figure 3. TEM image of the cross section of the coating and its elemental mapping (single-layer coating).

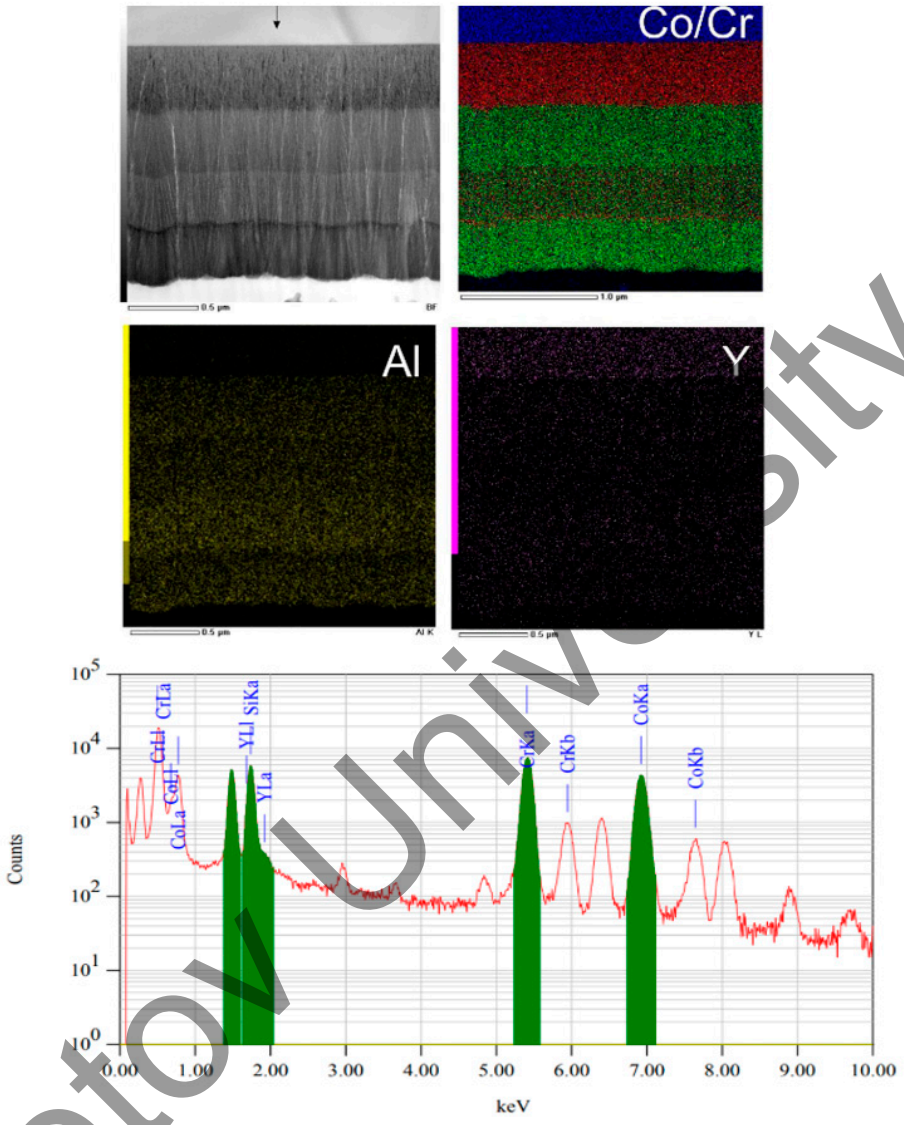

Figure 4. TEM image of the cross section of the coating and its elemental mapping (four-layer coating).

Table 4. Elemental analysis of composite coatings.

Sample	Elements, Mass%				
	Si	Al	Cr	Co	Y
Single-layer coating	5.49 ± 0.20	24.10 ± 0.04	30.98 ± 0.05	36.86 ± 0.05	2.58 ± 0.12
Four-layer coating	15.15 ± 0.07	13.12 ± 0.07	40.06 ± 0.04	30.29 ± 0.06	1.37 ± 0.63
Eight-layer coating	7.89 ± 0.14	13.03 ± 0.08	49.36 ± 0.03	28.14 ± 0.07	1.57 ± 0.41

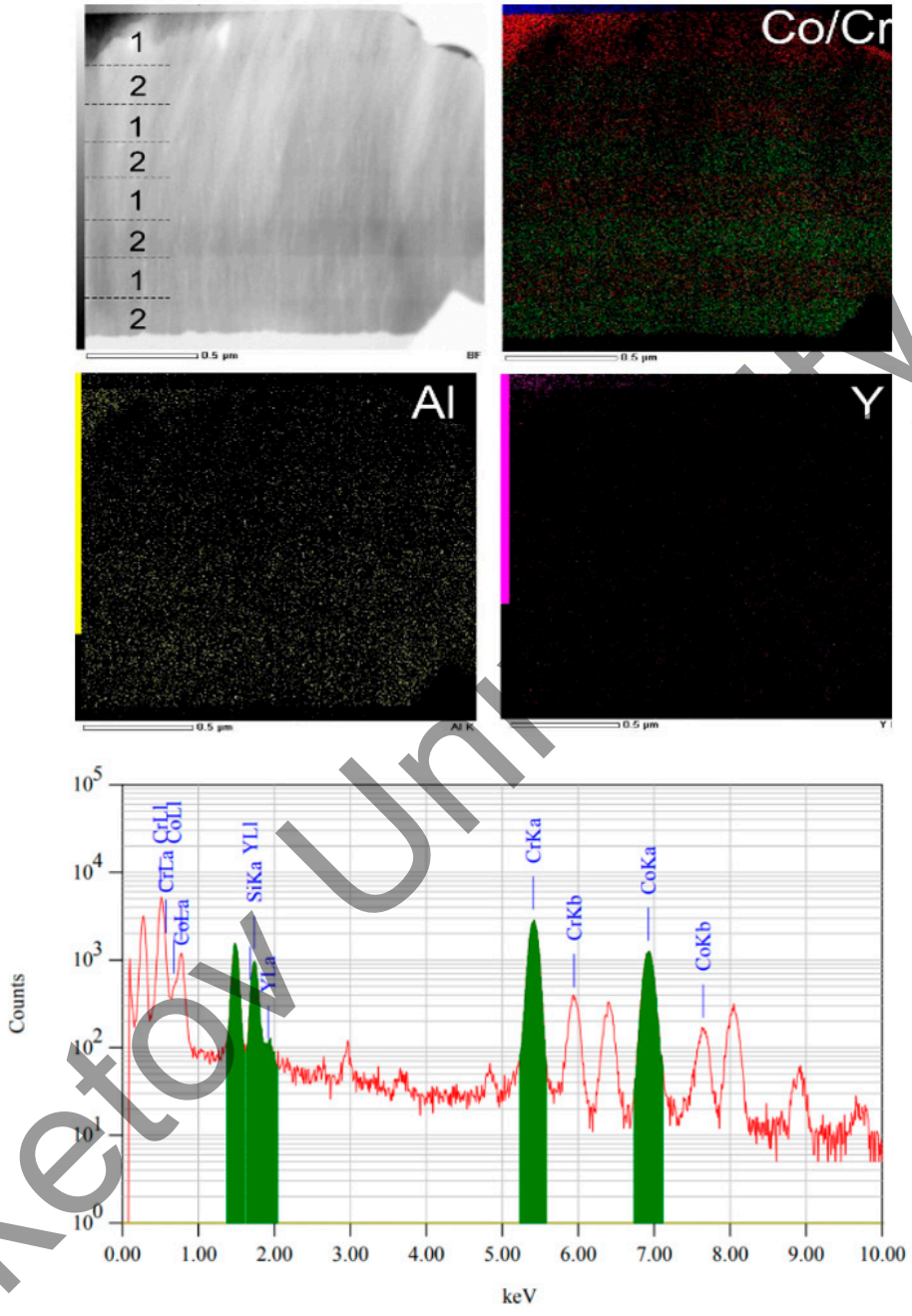

Figure 5. TEM image of the cross section of the coating and its elemental mapping (eight-layer coating).

Elemental mapping by constituent elements showed a relatively uniform distribution of Al and Y in the coating, the layers of enriched/depleted Co/Cr alternate in accordance with the parameters of magnetron sputtering.

The content of Co is a maximum of 36.86 ± 0.05% in the single-layer coating and a minimum of 28.14 ± 0.07% in the eight-layer coating. The chromium content, on the contrary, increases with the increase in the number of layers: in the single-layer coating—30.98 ± 0.05% and in the eight-layer coating—49.36 ± 0.03%. Aluminum is evenly distributed over all layers of the coating. Its content in the single-layer coating is 24.10 ± 0.04% and in the eight-layer coating—13.03 ± 0.08%. Yttrium is located in the form of a small thin layer at the film/substrate interface. During thinning using ion argon guns, it is etched away until destruction (EDS detects a weak peak merged with a large silicon peak).

A distinctive feature of the layers is the absence of a crystalline structure in some areas of the Co-Cr-Al-Y multilayer coatings, which is apparently due to the amorphous properties of cobalt and its tendency to form metallic glasses. Obtaining an amorphous state is primarily associated with nonequilibrium processes occurring during the formation of thin films. Since the amorphous state is metastable, when heated, it changes to a more stable crystalline state. In the vast majority of cases, the crystallization of the amorphous phase in metallic glasses occurs by the mechanism of nucleation and growth. The possibility of glass formation is determined by such factors as the rate of cooling and the frequency of nucleation of crystals [25,26].

EDS mapping in a sample of the eight-layer coating showed that the concentration of Co increases closer to the substrate; apparently, an incompletely controlled process of film growth is observed.

The results of the X-ray diffraction phase analysis of the coatings in the initial state by the gliding beam method are shown in Figure 6.

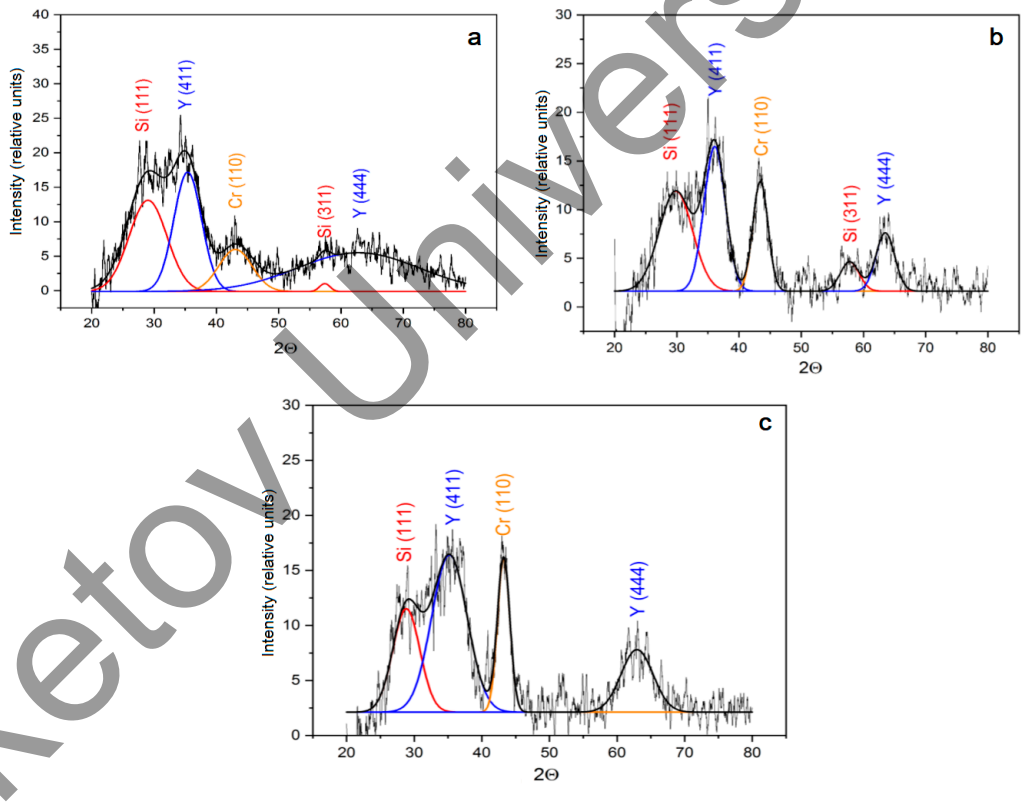

Figure 6. X-ray diffraction phase analysis results: (**a**) single-layer coating; (**b**) four-layer coating; (**c**) eight-layer coating.

The results of X-ray diffraction phase analysis for all Co-Cr-Al-Y coatings in the initial state show that the main peaks can be distinguished on the X-ray patterns: $2\theta \approx 30^\circ$ and 57°, corresponding to the first and third order peaks of the silicon substrate (111) (Table 5). The dominant Cr (110) peak at $2\theta \approx 43^\circ$ is pronounced for multilayer coatings and much less intense for single-layer coating. This correlates with the significantly lower Cr concentration in the single-layer coating measured from the EDS results. Fourth-order peaks Y (411) and Y (444) are also present.

The absence of Co and Al peaks is probably because they form an X-ray amorphous layer, which is confirmed by the results of transmission microscopy. Summing up the results of TEM and XRD, we can state the formation of an amorphous Co/Al matrix with Cr and Y nanocrystals distributed in the coating. No formation of intermetallic compounds in the deposited Co-Cr-Al-Y system was found.

Table 5. Results of XRD phase analysis.

Sample	Intensity, Rel. Units	2θ, °	Peak (hkl)
Single-layer coating	13	30	Si (111)
	17	36	Y (411)
	5	44	Cr (110)
	5	63	Y (444)
	1	57	Si (311)
Double-layer coating	19	30	Si (111)
	25	38	Y (411)
	24	44	Cr (110)
	10	64	Y (444)
	5	56	Si (311)
Four-layer coating	13	30	Si (111)
	17	36	Y (411)
	13	43	Cr (110)
	13	65	Y (444)
	5	57	Si (311)
Eight-layer coating	12	30	Si (111)
	17	35	Y (411)
	17	44	Cr (110)
	7	63	Y (444)

The diffraction pattern of the single-layer coating sample in the asymmetric geometry mode is shown in Figure 7. In the case of using asymmetric geometry, the angle between the sample surface and the X-ray beam was changed in the range of 1–5°, to analyze the material layer by layer. The step during the study was 0.05°, and the accumulation time was 3 s at each point. Clear reflections in the symmetric geometry (Bragg–Brentano), with the exception of the silicon substrate reflection 111, were not observed. The transition to asymmetric imaging geometry also did not allow detecting the peaks of crystalline phases, with the exception of substrate silicon, based on which it was also concluded that the coatings were amorphous in their initial state.

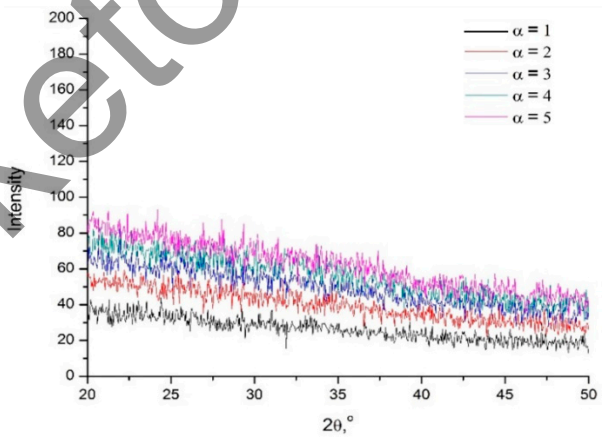

Figure 7. X-ray diffraction pattern of the single-layer Co-Al-Cr-Y coating in asymmetric geometry mode.

For the multilayer Co-Al-Cr-Y sample, some features are observed. On the X-ray pattern, reflections of polycrystalline phases were noticed, which do not belong to silicon and clearly belong to other phases (Figure 8). The transition to asymmetric geometry also confirmed the presence of these peaks. Phase analysis showed the three most suitable candidates based on the positions of the reflections are Co_3O_4 (d = 2.4716 Å), $AlSi_{0.5}O_{2.5}$ (d = 3.79 Å) and SiO_2 (d = 4.21 Å). The formation of all these phases, apparently, can be associated with the interaction of the substrate, the film substance and the environment

during the preparation of the composite. Silicon dioxide, in particular, could form on the surface of the single-crystal substrate prior to film deposition.

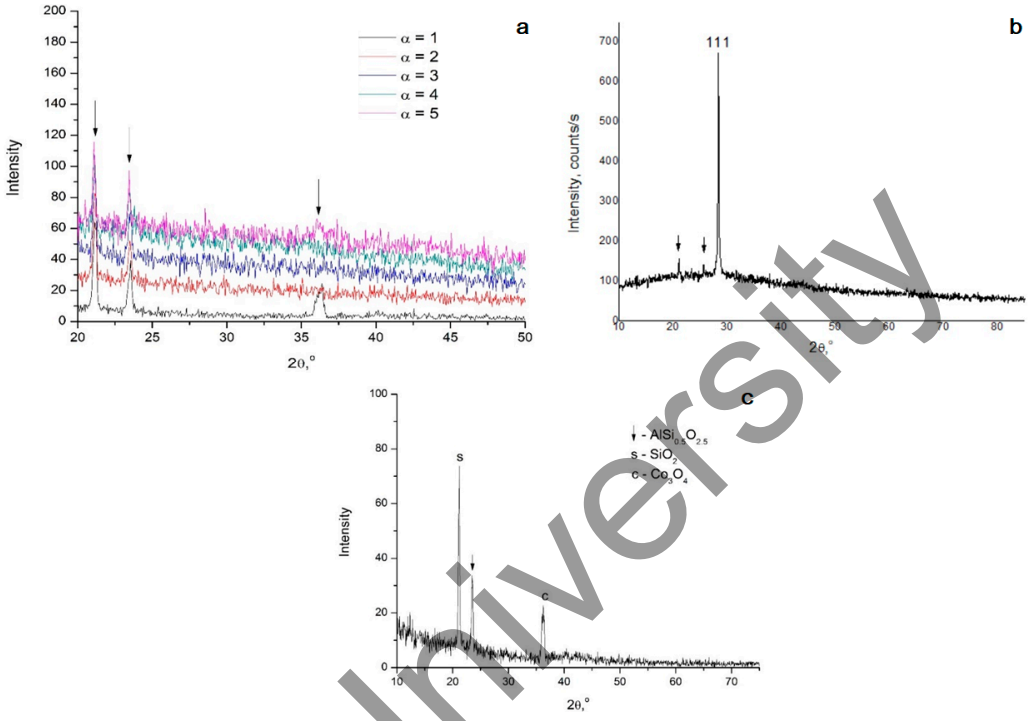

Figure 8. X-ray diffraction pattern of the multilayer Co-Al-Cr-Y coating: (**a**) in normal mode; (**b**) in asymmetric geometry at different angles; (**c**) in asymmetric geometry at $\alpha = 1°$.

The surface morphology of single-layer and multilayer Co-Cr-Al-Y coatings is shown in Figure 9. AFM results of all coatings correlate with SEM measurements. The average roughness Ra for all samples is in the range of 16–27 μm (the initial roughness of the Si substrate is 2.5 μm), without a strict dependence on the number of layers, which is probably due to the amorphous structure of the coatings. The peak roughness of coatings, Szmax, is due to rare inclusions and melting of part of the sprayed material.

To reveal the effect of temperature on the structural-phase state and properties of the coatings, the samples were heated up to 400 °C, 800 °C and 1000 °C.

For samples after heat treatment at 400 °C, some changes are noticed using XRD. In the case of the single-layer sample, it was not possible to fix extraneous reflections except for the reflections of the silicon substrate 111 and 220 (Figure 10a). These reflections are mainly due to the defocus of the incident beam on the sample when it is incident at small angles.

However, for the rest of the samples, the appearance of reflections of a number of phases was noticed, such as: SiO_2, CoO, $AlSi_{0.5}O_{2.5}$ and $CrAl_{0.42}Si_{1.58}$ (Figure 10b).

Further increase in the treatment temperature to 800°C does not lead to significant changes. In the case of the multilayer sample, the reflections of various impurity phases disappeared and the Co_3O_4 phase formed (Figure 11). It should be noted that the $CoCr_2O_4$ phase, which also has a spinel-type structure, has a similar set of reflections in position and intensity, and elemental analysis data showed a homogeneous distribution of the elements in the material.

For samples treated at 1000 °C, the formation of a spinel-type phase (Co_3O_4-$CoCr_2O_4$) was observed in all cases. In the sample with eight layers, impurities were also found similar to those observed at lower temperatures but were not observed for the sample treated at 800 °C. In this case, this is because the samples had different areas and, therefore, contained different amounts of the substance, based on which the reflections of impurity phases could not be observed in the case of one sample, but the phases themselves could

be preserved. In the case of the four-layer coating, the yttrium oxide phase was found (Figure 12). Results of XRD phase analysis after heat treatment are summarized in Table 6.

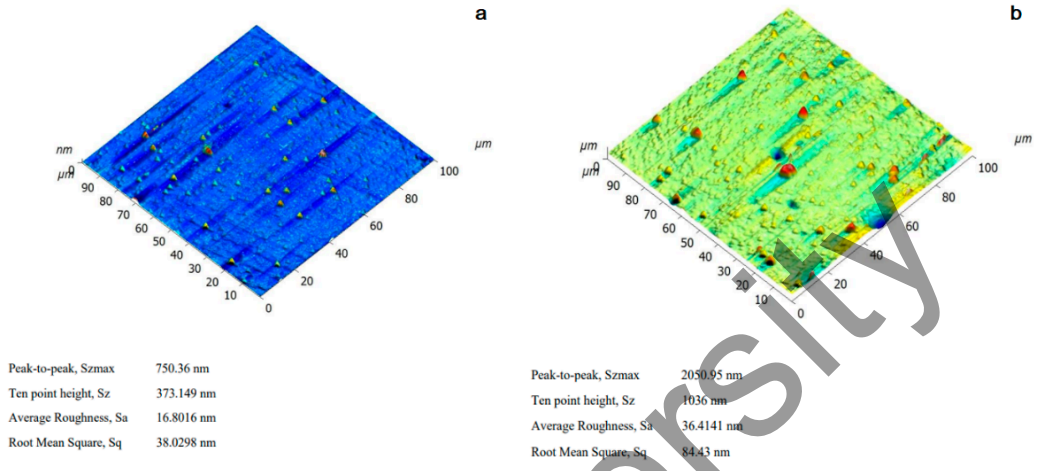

Figure 9. Surface morphology of the single-layer (**a**) and multilayer (**b**) Co-Cr-Al-Y coating.

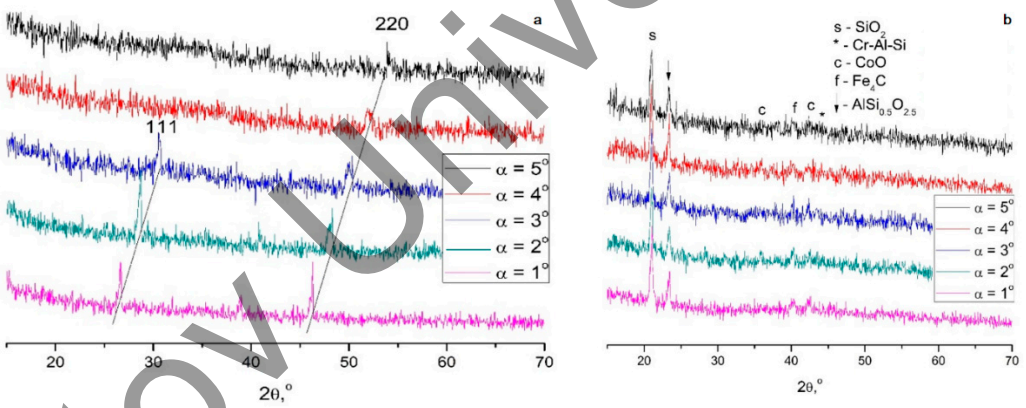

Figure 10. Diffractograms of single-layer (**a**) and multilayer (**b**) Co-Al-Cr-Y coatings in asymmetric geometry after heat treatment at 400 °C.

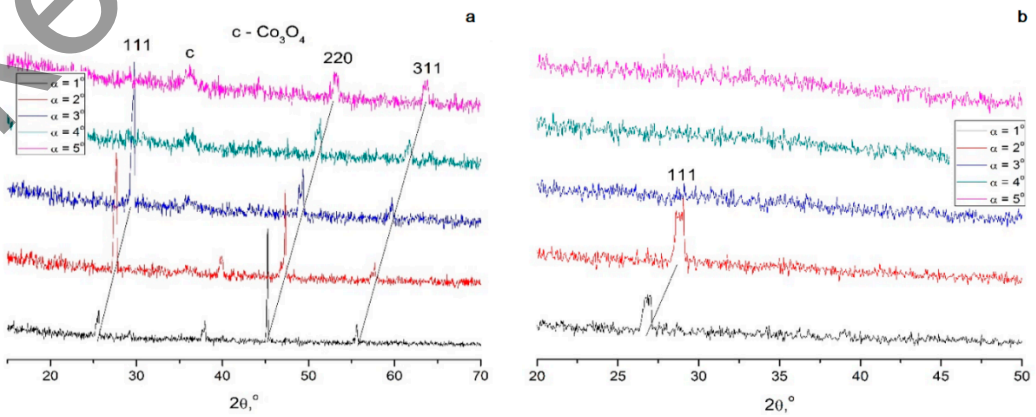

Figure 11. X-ray diffraction patterns of four-layer (**a**) and eight-layer (**b**) Co-Al-Cr-Y coatings in asymmetric geometry after heat treatment at 800 °C.

Table 6. Phases revealed as a result of X-ray diffraction phase analysis after heat treatment.

Sample	Phase
2-, 4-, 8-layer coating (400 °C)	SiO_2
2-, 4-, 8-layer coating (400 °C)	CoO
2-, 4-, 8-layer coating (400 °C)	$AlSi_{0.5}O_{2.5}$
2-, 4-, 8-layer coating (400 °C)	$CrAl_{0.42}Si_{1.58}$
4-, 8-layer coating (800 °C)	Co_3O_4
8-layer coating (800 °C), 4-, 8-layer coating (1000 °C)	Y_2O_3
1-, 2-, 4-, 8-layer coating (400 °C)	Co_3O_4–$CoCr_2O_4$

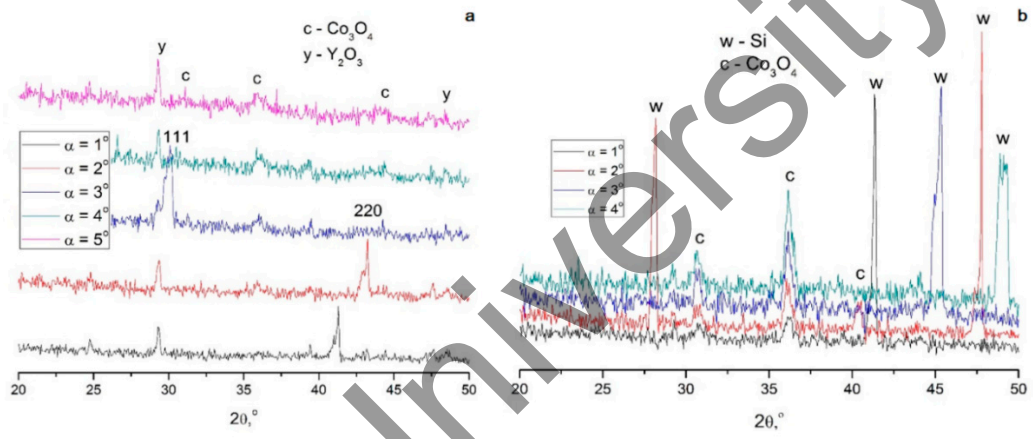

Figure 12. X-ray diffraction patterns of the four-layer (**a**) and eight-layer (**b**) Co-Al-Cr-Y coating in asymmetric geometry after heat treatment at 1000 °C.

The main process occurring during heat treatment of multilayer composites is the formation of a spinel-type phase. In this case, despite the symbol Co_3O_4, the composition of the resulting spinel may be different and may include Cr, Y and Al, based on the possible charge states of these cations (Cr^{3+}, Al^{3+}, Y^{3+}). Their final formation for all samples occurs in the temperature range of 800–1000°C. In this case, the yttrium oxide phase can form separately from particles with this structure, which is due to the large size of the Y^{3+} cations.

The possible reason for the formation of spinel structures is the strong acidification of the films, which was also demonstrated for the initial amorphous samples by the TEM method. The fairly uniform nature of the saturation of the layers with oxygen indicates that the samples were acidified at the stage of their deposition onto the substrate. Apparently, the heat treatment of the samples leads not to the reduction of oxides, but to their crystallization. This means that in the future, to obtain composite metal layers by heat treatment, it is necessary to use a medium with a more reducing character, for example, Ar/H_2 or He/H_2, which will facilitate the process of reduction of the original spinels.

Figure 13 shows the surface morphology of four-layer and eight-layer Co-Cr-Al-Y coating after heat treatment at 800 °C. The average roughness Ra for all samples changed (14.7–25.3 μm), in comparison with the average roughness of the samples before heat treatment (16.0–36.0 μm). Accordingly, the peak roughness of the coatings Szmax after heat treatment is also lower. Table 7 summarizes the obtained results.

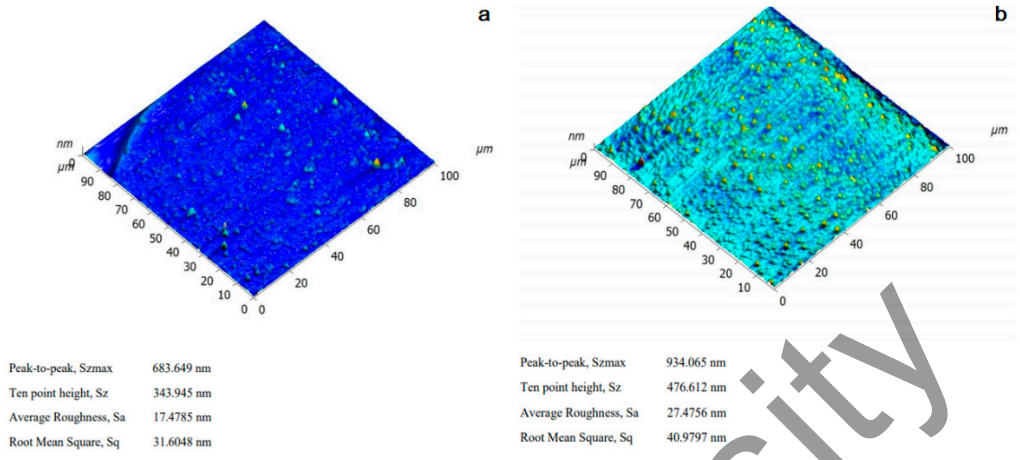

Figure 13. Surface morphology of four-layer and eight-layer Co-Cr-Al-Y coatings after heat treatment at 800 °C.

Table 7. Averaged Ra, Rz of Cr-Al-Co-Y coating surface after heat treatment.

Samples Treated at 400 °C	R_a, μm	R_z, μm	Samples Treated at 800 °C	R_a, μm	R_z, μm	Samples Treated at 1000 °C	R_a, μm	R_z, μm
Single-layer coating	18.4	125.6	Single-layer coating	18.1	125.6	Single-layer coating	17.1	125.6
Double-layer coating	16.5	120.0	Double-layer coating	16.0	120.0	Double-layer coating	15.3	120.0
Four-layer coating	25.3	133.1	Four-layer coating	25.1	133.1	Four-layer coating	24.8	133.1
Eight-layer coating	15.6	99.5	Eight-layer coating	15.1	99.5	Eight-layer coating	14.7	99.5

The heat-treated Co-Cr-Al-Y coatings practically did not change the hardness values compared to the untreated samples (4.7–6.4 GPa) (Figure 14, Table 8).

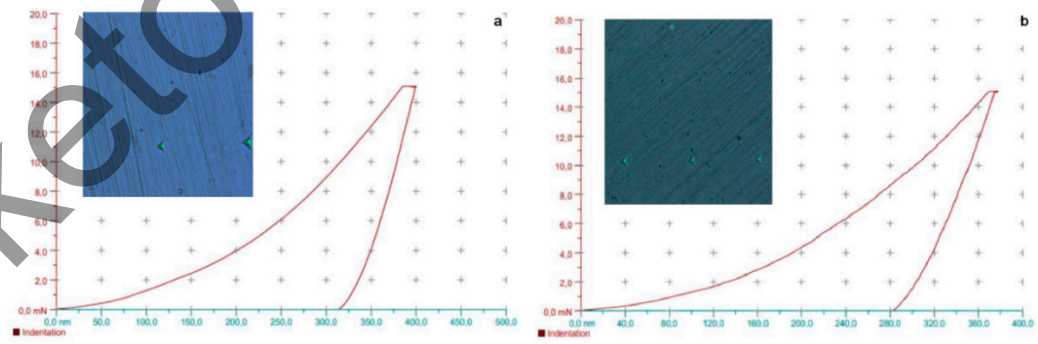

Figure 14. Loading curve for samples of four-layer (**a**) and eight-layer (**b**) coatings after heat treatment at 800 °C.

Table 8. Microhardness of the samples after heat treatment.

Samples Treated at 400 °C	Microhardness, GPa	Samples Treated at 800 °C	Microhardness, GPa	Samples Treated at 1000 °C	Microhardness, GPa
Single-layer coating	5.80 ± 0.11	Single-layer coating	5.90 ± 0.11	Single-layer coating	5.70 ± 0.11
Double-layer coating	6.60 ± 0.10	Double-layer coating	6.60 ± 0.10	Double-layer coating	6.40 ± 0.10
Four-layer coating	6.70 ± 0.10	Four-layer coating	7.00 ± 0.10	Four-layer coating	6.60 ± 0.10
Eight-layer coating	4.90 ± 0.09	Eight-layer coating	5.20 ± 0.09	Eight-layer coating	4.90 ± 0.09

The microstructure of the samples treated at 400 °C is shown in Figure 15. The structure of the samples, as well as that of the untreated ones, is columnar and microcracks are observed. The layers are clearly distinguishable on the TEM, STEM images and EDS maps (Figure 16).

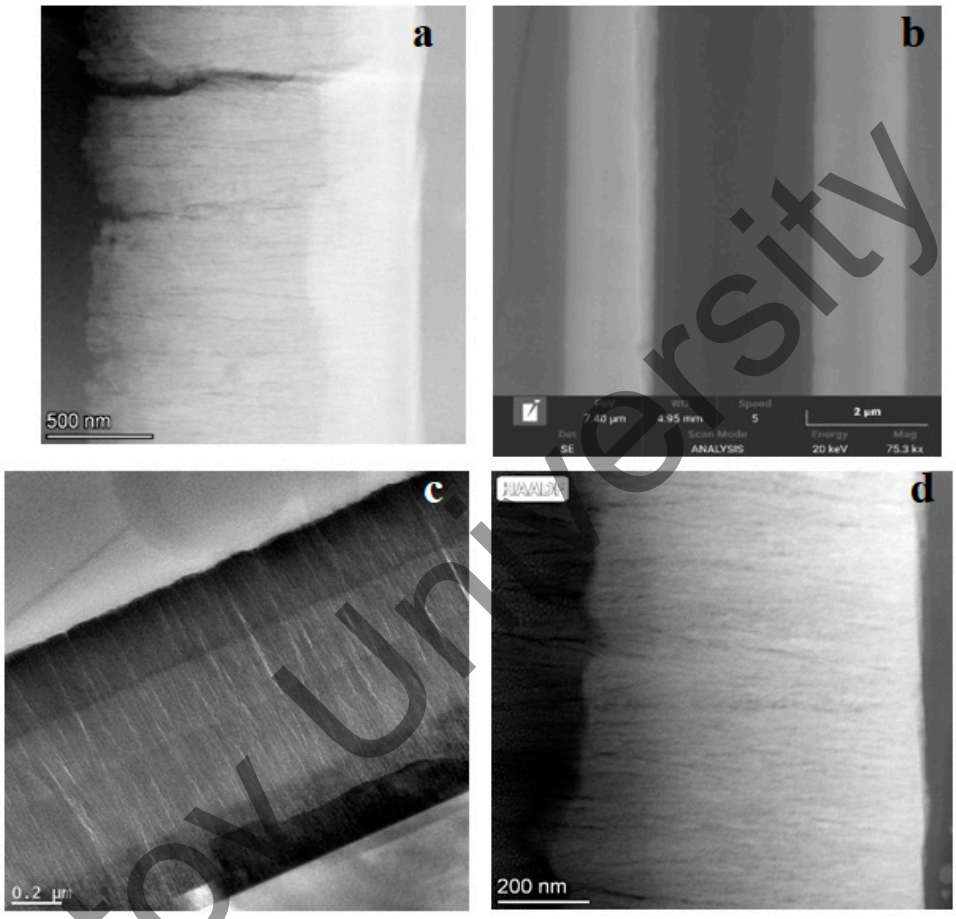

Figure 15. Microstructure of samples treated at 400 °C: (**a**) single-layer; (**b**) double-layer; (**c**) four-layer; (**d**) eight-layer coatings.

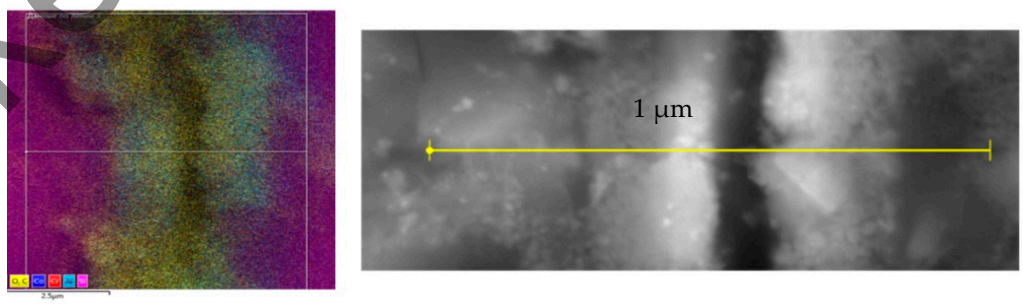

Figure 16. EDS analysis of the double-layer coating at 1000°C.

The structure of the samples heated at 1000 °C is shown in Figure 17. The structure is similar to all previous samples; the presence of layers is clearly distinguishable in all modes of TEM and SEM. As with the previous samples, the mixing of the film layers is noticeable.

The structure is similar to all previous samples; the presence of layers is clearly distinguishable in all modes of TEM (also SEM). As with the previous heated samples, mixing of the coating layers is observed. According to the mapping results, the silicon content in the coatings after heat treatment increased significantly—more than 10 times. For example, for single-layer coating (400 °C) it was 29.52% and for double-layer coating

(400 °C)—33.10%. It was observed that the cobalt content decreases with increasing heating temperature. Thus, for one-, two-, four- and eight-layer coatings heated at 400 °C, the cobalt content is 31.30, 17.10, 7.57 and 3.58%, respectively. For one-, two-, four- and eight-layer coatings at 800 °C, the cobalt content is 4.00, 19.91, 4.50 and 10.37%, respectively. Aluminum is distributed evenly over all layers of the coating. The maximum content of Al was in single-layer coatings subjected to heat treatment at temperatures of 400 and 1000 °C. The minimum value for the Al content was in the eight-layer coating (400 °C)—1.49%. In the remaining samples, this value ranges from 3.60 to 8.22%. Chromium and cobalt are distributed in a gradient. The average value of the chromium content is generally similar to samples without heat treatment. However, it was found that for eight-layer (400 °C), single-layer (800 °C) and double-layer (1000 °C) coatings, the chromium content is 1.38, 3.20 and 4.60%, respectively. After heat treatment, it was possible to establish the following content of Y: in single-layer (400 °C)—0.72%, in eight-layer (400 °C)—0.04%, in single-layer (1000 °C)—0.97%, in four-layer (1000 °C)—0.32% and in eight-layer (1000 °C)—0.52%.

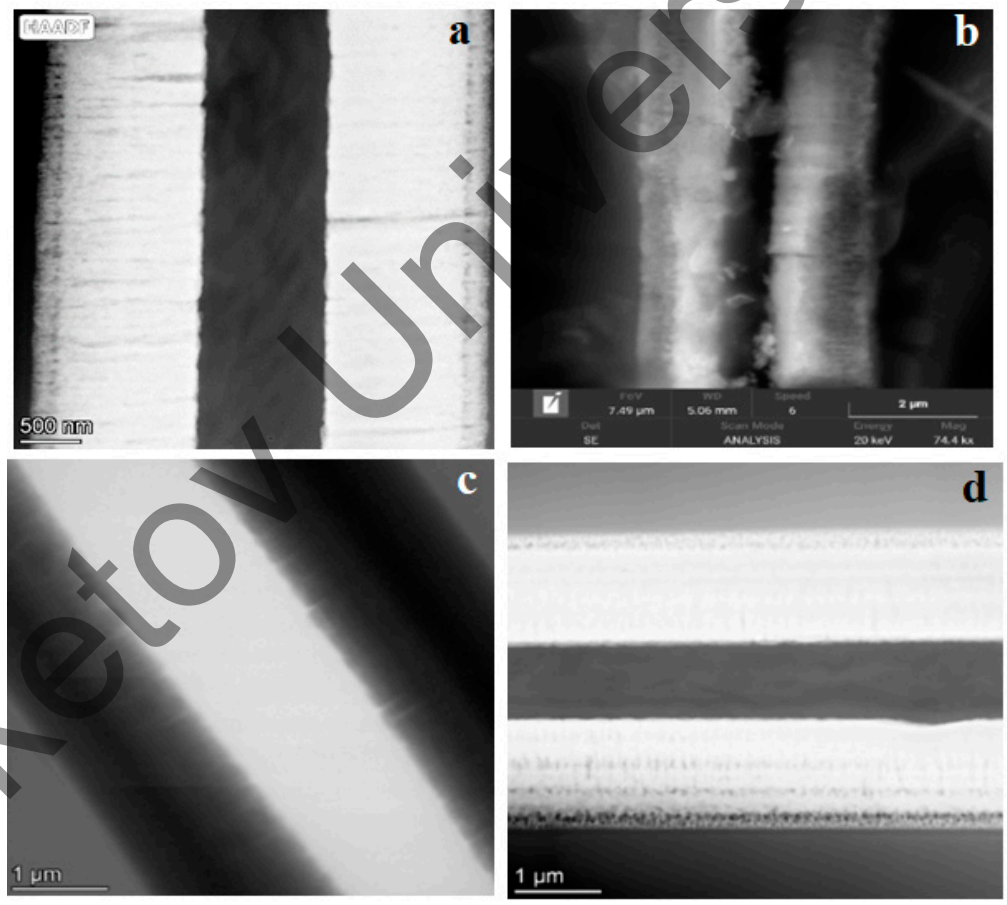

Figure 17. Structure of samples heated at 1000 °C: (**a**) single-layer; (**b**) double-layer; (**c**) four-layer; (**d**) eight-layer coatings.

At the heating temperature of 400 °C, the oxygen content in single- and eight-layer coatings was not established, similarly for single- and four-layer coatings at 1000 °C. The oxygen content in double- and four-layer coatings was 25.80 and 45.82%, respectively. As noted above, the presence of oxygen in the surface layer of the coatings is due to its adsorption on the cut surface after removal from the vacuum chamber.

All layers on each sample are clearly distinguishable, but the distribution of elements in the composition has a gradient character. In some of the images, the coating is slightly destroyed, which is a consequence of ion etching, since the substrate is etched faster than the coating. All samples have a columnar structure; at high magnifications, small cracks

were seen in the upper layers, which then "go" deeper, which is evidence of the presence of microstresses in the sample, while etching revealed the presence of microstresses.

4. Conclusions

The structural-phase state and properties of multilayer Co-Cr-Al-Y coatings on a single-crystal silicon substrate, obtained using a magnetron system with dual magnetrons, have been studied. The thickness of all obtained Co-Cr-Al-Y coatings ranges from 1.5–1.7 ± 0.2 μm.

Coatings in the initial state are characterized by a hardness value in the range of 4.7–6.4 GPa. At the same time, the value of H/E is non-linear with a maximum for a four-layer coating of 0.048, which makes it the most crack-resistant system of all those studied.

SEM studies made it possible to establish that the Co-Cr-Al-Y system forms coatings with a textured structure. Transmission microscopy results confirm the SEM and EDS measurements. A distinctive feature of the synthesized layers is the almost complete absence of a crystalline structure, which is associated with the amorphous properties of cobalt and its tendency to form metallic glasses.

Thus, it was found that the coating in the initial state has a characteristic layered structure. Crystallization of the coating during sputtering proceeds in the form of crystallized particles. Zones of columnar crystals are distinguished in such particles.

According to the data of X-ray diffraction phase analysis, identical data on amorphism were revealed. Samples of multilayer coatings in the initial state are predominantly X-ray amorphous. No clear reflections were observed in the symmetric geometry, and the transition to the asymmetric geometry did not allow detection of the peaks of crystalline phases, with the exception of substrate silicon.

The main process occurring during heat treatment (400, 800 and 1000 °C) of the studied composites is the formation of a spinel-type phase. In this case, despite the symbol Co_3O_4, the composition of the resulting spinel may be different and may include Cr, Y and Al, based on the possible charge states of these cations (Cr^{3+}, Al^{3+}, Y^{3+}). Their final formation for all samples occurs in the temperature range of 800–1000 °C. In this case, the yttrium oxide phase can form separately from particles with this structure, which is due to the large size of the Y^{3+} cations.

Heating affected the internal structure of the samples. All layers on each sample are clearly distinguishable, but the distribution of elements in the composition has a gradient character. Small cracks were also noticed in the upper layers, which then "go" deeper, which is evidence of the presence of microstresses in the sample. The average values of the hardness of the heat-treated coatings practically did not change.

Data on the structural-phase state and properties of the multilayer Co-Cr-Al-Y coating can be used to predict the nature of such coatings after heat treatment.

Author Contributions: Conceptualization, M.S. and A.Z. (Almira Zhilkashinova); methodology, A.Z. (Assel Zhilkashinova) and M.A. (Madi Abilev); validation, M.S., A.Z. (Assel Zhilkashinova), A.Z. (Almira Zhilkashinova) and M.A. (Maksut Agelmenev); investigation, A.Z. (Assel Zhilkashinova), A.Z. (Almira Zhilkashinova), M.A. (Madi Abilev) and A.I.; resources, A.Z. (Almira Zhilkashinova), N.P. and A.I.; data curation, A.Z. (Assel Zhilkashinova), A.Z. (Almira Zhilkashinova) and M.A. (Maksut Agelmenev); writing—original draft preparation, A.Z. (Almira Zhilkashinova) and M.A. (Madi Abilev); writing—review and editing, M.S., A.Z. (Almira Zhilkashinova), M.A. (Madi Abilev) and M.A. (Maksut Agelmenev); visualization, M.A. (Madi Abilev) and M.A. (Maksut Agelmenev); supervision, M.S. and A.Z. (Almira Zhilkashinova); project administration, A.Z. (Almira Zhilkashinova) and N.P.; funding acquisition, A.Z. (Almira Zhilkashinova) and N.P. All authors have read and agreed to the published version of the manuscript.

Funding: This research was funded by the Science Committee of the Ministry of Education and Science of the Republic of Kazakhstan, grant number AP08053322 and Education, Audiovisual, and Culture Executive Agency, grant number 543746.

Institutional Review Board Statement: Not applicable.

Informed Consent Statement: Not applicable.

Data Availability Statement: Not applicable.

Conflicts of Interest: The authors declare no conflict of interest.

References

1. Wang, L.; Zhong, X.; Zhao, Y.; Tao, S.; Zhang, W.; Wang, Y.; Sun, X. Design and optimization of coating structure for the thermal barrier coatings fabricated by atmospheric plasma spraying via finite element method. *J. Asian Ceram. Soc.* **2014**, *2*, 102–116. [CrossRef]
2. Lu, Z.; Myoung, S.; Kim, E.; Lee, J.; Jung, Y. Microstructure Evolution and Thermal Durability with Coating Thickness in APS Thermal Barrier Coatings. *Mater. Today Proc.* **2014**, *1*, 35–43. [CrossRef]
3. Feuerstein, A.; Knapp, J.; Taylor, T.; Ashary, A.; Bolcavage, A.; Hitchman, N. Technical and Economical Aspects of Current Thermal Barrier Coating Systems for Gas Turbine Engines by Thermal Spray and EBPVD: A Review. *J. Therm. Spray Technol.* **2008**, *17*, 199–213. [CrossRef]
4. Chen, P.; Wang, S.; Wang, F.-H. Fracture Analysis of Thermal Barrier Coating Delamination under Thermal Shock. *Procedia Eng.* **2015**, *99*, 344–348. [CrossRef]
5. Belmonte, M. Advanced Ceramic Materials for High Temperature Applications. *Adv. Eng. Mater.* **2006**, *8*, 693–703. [CrossRef]
6. Clarke, D.R.; Phillpot, S.R. Thermal barrier coating materials. *Mater. Today* **2005**, *8*, 22–29. [CrossRef]
7. Vaßen, R.; Jarligo, M.O.; Steinke, T.; Mack, D.E.; Stöver, D. Overview on advanced thermal barrier coatings. *Surf. Coat. Technol.* **2010**, *205*, 938–942. [CrossRef]
8. Marino, K.A.; Hinnemann, B.; Carter, E.A. Atomic-scale insight and design principles for turbine engine thermal barrier coatings from theory. *Proc. Natl. Acad. Sci. USA* **2011**, *108*, 5480–5487. [CrossRef]
9. Tailor, S.; Mohanty, R.M.; Doub, A.V. Development of a new TBC system for more efficient gas turbine engine application. *Mater. Today Proc.* **2016**, *3*, 2725–2734. [CrossRef]
10. Konter, M.; Bossmann, H.-P. Materials and coatings developments for gas turbine systems and components. In *Modern Gas Turbine Systems*; Hughes, S., Ed.; Woodhead Publishing Limited: Cambridge, UK, 2013; pp. 327–381e. [CrossRef]
11. Bala, N.; Singh, H.; Prakash, S. Performance of cold sprayed Ni based coatings in actual boiler environment. *Surf. Coat. Technol.* **2017**, *318*, 50–61. [CrossRef]
12. Drory, M.D.; Evans, R.D. Deposition and characteristics of chromium nitride thin film coatings on precision balls for tribological applications. *Surf. Coat. Technol.* **2011**, *206*, 1983–1989. [CrossRef]
13. Chetcuti, R.; Dearnley, P.A.; Mazzonello, A.; Buhagiar, J.; Mallia, B. Tribocorrosion response of duplex layered CoCrMoC/CrN and CrN/CoCrMoC coatings on implant grade 316LVM stainless steel. *Surf. Coat. Technol.* **2020**, *384*, 125313. [CrossRef]
14. Alinezhadfar, M.; Abad, S.N.K.; Mozammel, M. Multifunctional cobalt coating with exceptional amphiphobic properties: Self-cleaning and corrosion inhibition. *Surf. Interfaces* **2020**, *21*, 100744. [CrossRef]
15. Rakoch, A.G.; Van Tuan, T.; Khabibullina, Z.V.; Blawert, C.; Serdechnova, M.; Scharnagl, N.; Zheludkevich, M.L.; Gladkova, A.A. Role of cobalt additive on formation and anticorrosion properties of PEO coatings on AA2024 alloy in alkali-silicate electrolyte. *Surf. Coat. Technol.* **2022**, *433*, 128075. [CrossRef]
16. Soumya, S.S.; Xavier, T.S. Effect of cobalt doping on the microstructural, optical and electrical properties of SnO_2 thin films by sol-gel spin coating technique. *Phys. B Condens. Matter* **2022**, *624*, 413432. [CrossRef]
17. Lashmi, P.G.; Ananthapadmanabhan, P.V.; Unnikrishnan, G.; Aruna, S. Present status and future prospects of plasma sprayed multilayered thermal barrier coating systems. *J. Eur. Ceram. Soc.* **2020**, *40*, 2731–2745. [CrossRef]
18. Fu, Q.; Tietz, F.; Sebold, D.; Wessel, E.; Buchkremer, H.-P. Magnetron-sputtered cobalt-based protective coatings on ferritic steels for solid oxide fuel cell interconnect applications. *Corros. Sci.* **2012**, *54*, 68–76. [CrossRef]
19. Sarakinos, K.; Alami, J.; Konstantinidis, S. High power pulsed magnetron sputtering: A review on scientific and engineering state of the art. *Surf. Coat. Technol.* **2010**, *204*, 1661–1684. [CrossRef]
20. Medvedovski, E.; Mendoza, G.L.; Rzad, E.; Solecka, M.; Dudziak, T.P. Influence of multi-layered thermal diffusion coatings on high-temperature sulfidation resistance of steels. *Surf. Coat. Technol.* **2020**, *403*, 126430. [CrossRef]
21. Luo, H.; Li, X.; Pan, C.; He, P.; Zeng, K.; Hu, K.; Li, H.; Yang, C. Microstructure and oxidation resistance of CoNiCrAlY coating manufactured by laser powder bed fusion. *Surf. Coat. Technol.* **2021**, *427*, 127846. [CrossRef]
22. Mardanifar, A.; Mohseni, A.; Mahdavi, S. Wear and corrosion of Co-Cr coatings electrodeposited from a trivalent chromium solution: Effect of heat treatment temperature. *Surf. Coat. Technol.* **2021**, *422*, 127535. [CrossRef]
23. Meng, G.-H.; Liu, H.; Xu, P.-Y.; Li, G.-R.; Xu, T.; Yang, G.-J.; Li, C.-J. Superior oxidation resistant MCrAlY bond coats prepared by controlled atmosphere heat treatment. *Corros. Sci.* **2020**, *170*, 108653. [CrossRef]
24. Zhilkashinova, A.; Abilev, M.; Pavlov, A.; Prokhorenkova, N.; Skakov, M.; Gradoboev, A.; Zhilkashinova, A. Ion-Plasma Spraying and Electron-Beam Treatment of Composite Cr-Al-Co-ZrO_2-Y_2O_3 Coating on the Surface of Ni-Cr Alloy. *Coatings* **2021**, *11*, 321. [CrossRef]
25. Telford, M. The case for bulk metallic glass. *Mater. Today* **2004**, *7*, 36–43. [CrossRef]
26. Petrzhik, M.I.; Vakaev, P.V.; Chueva, T.R.; Sviridova, T.; Molokanov, V.; Kovneristy, Y.; Levashov, E. From Bulk Metallic Glasses to Amorphous Metallic Coatings. *J. Metastable Nanocryst. Mater.* **2005**, *24–25*, 101–104. [CrossRef]